ARCHIVE OF MECHANICAL ENGINEERING

DOI: 10.24425/ame.2022.141524 2022, Vol. 69, No. 4, pp. 729–747

Hussein M. SALIH [1]

A comparative study for double pass solar air collector utilizing medial glass panel

Received 23 February 2022, **Revised** 28 June 2022, **Accepted** 1 July 2022, **Published online** 4 November 2022

Keywords: solar air collector, double-pass, CFD, finite volume, thermal performance

A numerical investigation of thermal prediction of double-pass solar air heater of-counter flow is developed in the present study. The main idea of the current study is that the collector consists of two layers of glass so that the middle layer is glass instead of the usual metal plate. The performance of double-pass solar air heater is studied for a wide range of solar radiation intensities (600, 750 and 900 W/m^2). A FORTRAN-90 program is built to simulate the mathematical model of double-pass solar air heater based on solving steady state two-dimensional Navier-Stokes equations and energy equation based on finite volume method. Turbulence effect is simulated by two equations k-ε module. The results are compared with the results of a previous experimental study and a good agreement was found. From compression calculating efficiency of the present and traditional collector for each solar intensity, it was found that the efficiency of the current collector is higher than that of the traditional one, where the efficiency of the current collector at the solar intensity of (600, 750 and 900) W/m^2 are (0.529, 0.514 and 0.503), respectively, while those of the traditional collector (0.508, 0.492 and 0.481), respectively. In addition to this, the effect of the mass flow rate on the temperature difference of the current proposed collector was studied. Three values of the mass flow rate were studied (0.009, 0.018, and 0.027) kg/s at solar intensity of 750 W/m^2. From this it was found that the temperature difference decreases with increasing mass flow rate. Accordingly, the efficiency decreases.

1. Introduction

In today's world, a large population growth coupled with industrial growth, have contributed to a global demand for energy, and this in effect has generated an interest in renewable energy, such as the sun as one of the most important sources

✉ Hussein M. Salih, e-mail: 50004@uotechology.edu.iq

[1] Electromechanical Engineering Department, University of Technology, Iraq. ORCID:0000-0002-9665-971X

of renewable energy, where electrical energy is generated through the conversion of solar energy into heat energy using solar collectors or photovoltaic panels. Solar air heaters are considered as simple, compact and cheap collectors, where incidental solar irradiation is converted into heat energy at the absorbing surface and then transferred to the air flowing by heat transfer by convection. Solar energy is used in many applications such as drying processes in addition to its use in space heaters and solar cookers [1–5]. One of the most important problems of using solar energy is low efficiency, which is one of the most important obstacles facing developers and workers in this field [6]. As a result, researches tend to find ways to increase and improve efficiency, and one of those researches is the present study. Assadeg et al. [7] introduced a matrix inversion method to solve energy balance for flow rate range of 0.01–0.15 kg/s, and solar irradiation range of (425–1000) W/m^2. The values of mass flow rate and solar irradiation on energy and exergy efficiency and the improvement potential have been estimated. Jalil and Shrooq [8] presented an experimental study of thermal efficiency of a lower channel of a double pass solar air collector consisting of a porous medium of stainless steel mesh and steel wool. Several types of porous media of high thermal conductivity and different porosities have been studied. Results showed that thermal efficiency with using porous media was greater than this without using it. Double waterway in vacuum tube technology has been used in new design, fabrication and performance inspection of parabolic trough by Bassem et al. [9]. This system can be used to raise the temperature of water in the winter without auxiliary devices. Jalil et al. [10] studied double-pass solar air heater with wavy fins absorber experimentally. The absorber was finned from upper and lower. The results showed an improvement in thermal efficiency in case of finned absorber compared with a normal absorber. Siddique et al. [11] presented an experimental study to improve the performance for different shapes of bottom wall utilizing ribs and corrugated wall of 26:5 aspect ratio SAH. The results noted that the best configurations were for collector of rectangular channel with ribs of staggered broken and trapezoidal corrugation at 45°. An analytical study of SAH with aid of arc-shaped ribs is presented by Ghritlahre [12]. Two different types of flow arrangement are studied: upstream and downstream flow. In addition, the SAH smooth duct was utilized in this study. Experiments were carried out using of 0.007–0.022 kg/s as mass flow rate range in Jamshedpur, India conditions. From the results, maximum thermal efficiency and exergy efficiency was 73.2% and 2.64%, respectively, for upstream flow at 0.022 kg/s, while maximum thermal and exergy efficiency was 69.4% and 1.89%, respectively, for downstream flow. Moreover, the results showed that the maximum exit temperature and temperature difference obtained at minimum mass flow rate. Kumar et al. [13] studied various designs of a double pass solar air heater and presented its thermal performance by utilizing a numerical model. The exit temperature was increased approximately five degrees when the absorber panel was located between the insulating wall and the outer glass cover. In addition, the use of asymmetric semi-circular rough surfaces instead of symmetric circular shapes shows better performance as re-attachment of

eddies to the absorber panel is more repeated in the previous condition. From this study, Nusselt number and friction factor were correlated as function of Reynolds number and relative roughness height. Abo-Elfadl et al. [14] proposed a new designed absorber. The performance of a double-pass solar air heater was studied experimentally. The new solar air heater absorber was made of aluminum tubes that are adjacent to each other and installed in the same direction as the air flow. The performance of the new solar air heater was studied with varying mass flow rates. The results were compared with those of a flat plat solar air heater of the same materials and dimensions except the absorber design. The results indicate that the new design has a higher air temperature at outlet, net energy gain, efficiency and top losses was lower than these in flat plat solar air heater. In addition, the efficiency of the proposed collector in the case of a double pass was greater than of a single pass. Energy balance and exergy equations for steady state condition for a new double pass solar air heater utilizing phase change materials and fins was investigated by Singh [15] who studied the double pass solar air heater experimentally and numerically. The collector was serpentine wavy wire-mesh packed bed. From the results, the efficiency was approximately 74% compared with those of a single pass solar air heater which was 57%. Ghritlahre and Sahu [16] presented a review study on energy analysis of different types of SAH and find out the research shortcoming for future study. Dogra and Sharma [17] developed a solar air heater by utilizing different geometries of ribs over the absorber plate, according to this; the performance of the collector can be enhanced as the result of increase in turbulence of flow and heat transfer coefficient and friction factor. It is also noted that using discrete ribs in place of continuous ribs gives more turbulence. Sivakumar et al. [18] presented an experimental study of thermodynamic analysis of a forced convection in a solar air heater utilizing pin-fins absorber. The results showed that the fin absorber improved the performance of the system with a minimum pressure drop across the air heater in comparison with the traditional one. The thermal performance of a double-pass solar air heater is investigated by Salih et al. [19]. PCM was used in the form of multiple rectangular capsules filled with paraffin wax. During charge/discharge process, an indoor projector simulator was used. In a mathematical part of the study, a numerical model based on finite-volume scheme SIMPLE algorithm was used. The study found that the increase in the air flow rate leads to a delay in the melting period and a decrease in the melting temperature of paraffin during melting period. Singh et al. [20] studied the performance of double-pass solar air heater of finned wire mesh with two glass covers experimentally. The results showed that the efficiency of a solar air heater reaches 80% maximum at air mass flow rate of 0.03 kg/s and solar intensity of 823 W/m^2. Saravanakumar et al. [21] developed an analytical study to improve the working of solar air heater by incorporating the rib into a jagged arc Fender with fins and baffles in the absorbent plate. The results showed that the proposed solar air heater increased the effectiveness and energy efficiency by 27.1% and 28.3%, respectively. Komolafe et al. [22] introduced an experimental study to predict

the performance of solar air heater utilizing rectangular rib roughness instead of absorber plate. The results show that the thermal efficiency range was 14.0–56.5%. Mzad et al. [23] presented a thermal performance of a trail solar air heater. The study showed that the enhancement of heat transfer within the air depends upon the selection of appropriate glass covers and efficient insulation materials. Patel and Lanjewar [24] presented an mathematical study of the performance of a W-shaped rough absorbent surface solar air heater using an analytical model and compared the results with a smooth-panel SAH for the same test conditions. Through the results, the researchers reached a maximum increase in the excessive efficiency of the zigzag rough surface SAH compared to the flat plate heater by 51%. An experimental study was presented for the thermal performance of a double-pass solar air heater by Mahmood [25] a phase change material (PCM) was used by filling a rectangular cavity with paraffin wax to obtain maximum performance during the evening hours and after sunset. Ravi and Saini [26] studied double pass solar air collector utilizing a V-shaped staggered rib. Results showed a significant increase in the Nusselt number and friction factor by 2.91–4.52, 2.08–3.13, and 2.91–4.52, respectively. Hassan and Abo-Elfadl [27] studied the effect of utilizing different configuration of absorber plate on the performance of a double pass solar air heater of two inlet ports. The effect of changing mass flow rate was studied for each configuration. Hosseini et al. [28] investigated a numerical study for natural convection of air inside solar air heaters utilizing elliptical, rectangular and triangular fins. A three-dimensional finite volume method was adopted; the realizable k-ε model was used for introducing the turbulence effect. Effect of tilt angle on mass flow rate and thermal performance of solar air heaters is introduced. The results showed little improvement in the thermal performance of solar air heaters with rectangular fins compared to those that contain two other shapes of fins of the same dimensions. Singh and Singh [29] presented a theoretical study for curved solar air heater performance. It was noticed that there is a slight rise in the pressure drop of the curved solar air heater compared with the flat one. A numerical study for thermal prediction of counter flow double-pass solar air heater was developed by Rasham and Alaskar [30]. The effect of absorber material and dimensions of air channels on the collector efficiency was studied. The results showed that there is an increase in the efficiency value of the collector of black plastic absorber plate over that of Aluminum absorber plate. Kumar and Chand [31] presented energy balance equations for the proposed corrugated Fins solar collector in steady state case. MATLAB was used to solve the model. The effect of fin pitch, fin spacing ratio, flow cross section aspect ratio and solar intensity on the thermal performance of the herringbone corrugated finned solar air heater was illustrated. Kareem et al. [32] studied two types of solar collector, single and double-pass utilizing porous media; metal chips or gravel as an absorbing medium. This article included a study of the parts of the solar collector and the materials used to manufacture, as well as the design of the collector and a study of its performance and uses. The study recommended the adoption of a multi-pass solar

collector for future applications. Fudholi et al. [33] developed a forced-convection flow in a double-pass solar air collector experimentally. The second channel of the collector was finned. The study concluded that the double-pass solar collector with finned absorber was more efficient than that of flat plate absorber by 8%. It also noticed that the efficiency of the collector depended significantly on the flow rate and the intensity of solar radiation. Theoretical and experimental studies of double pass solar air heater with and without porous material were presented by Ramani et al. [34]. A volumetric heat transfer coefficient was adopted in the mathematical model. Results showed that there was a significant increase in the efficiency of solar air heater with porous material compared to that of a traditional heater.

In the present study, a numerical study based on finite volume method will be developed to predict the flow behavior for a novel type of solar air heater. The present proposed collector consists of middle glass plate instead of the middle metal absorber.

Finally, after reviewing the previous literature, it can be noted that all the previous studies generally focused on the parametric study of the double-pass solar collector with a medial absorbent plate, while a new design is proposed by placing a middle glass plate and studying the impact of this on the performance of the collector, and here lies the novelty of the present study.

2. Physical domain

The collector consists of a double pass separated by a glass panel, and the outer cover is also made of glass. The length and width of each pass is 120 and 80 cm, respectively, with a height of 4 cm for each pass. The air passes through the upper passage and then through the gap to the lower passage to be sucked by the air blower with a mass flow rate of 0.009 kg/s. The thickness of each glass panel is 0.4 cm, while the absorber has a length, width and thickness of 120, 80 and 0.1 cm respectively. The counter-flow of the considered double-pass solar air collector and that of the traditional collector are shown in Fig. 1.

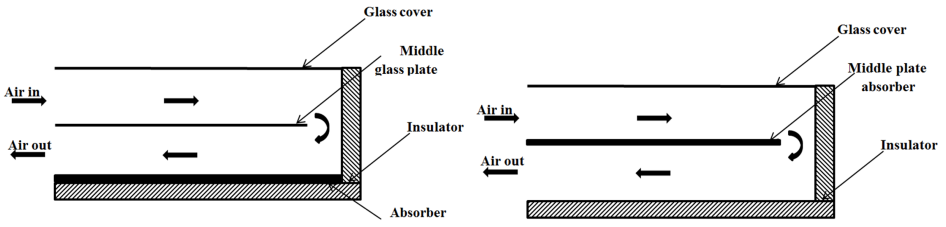

(a) proposed current collector (b) traditional collector

Fig. 1. Schematic diagram for solar air heater

3. Mathematical formulation

3.1. Numerical modeling for air flow within a collector

The mathematical model of the counter flow solar air collector based on the phenomenon of thermodynamic fluids is adopted. A numerical study of forced convection and heat transfer is modeled for an inclined duct. Simulations were accomplished by utilizing FORTRAN-90 program. The program was developed to solve three-dimensional partial differential Navier-Stokes equations and energy equation of the following form [35]:

1. Conservation of mass:

$$\frac{\partial(\rho u)}{\partial x}+\frac{\partial(\rho v)}{\partial y}+\frac{\partial(\rho w)}{\partial z}=0. \tag{1}$$

2. Conservation of momentum:

x momentum

$$\frac{\partial(\rho uu)}{\partial x}+\frac{\partial(\rho vu)}{\partial y}+\frac{\partial(\rho wu)}{\partial z}=-\frac{\partial p}{\partial x}+\frac{\partial}{\partial x}\left(2\mu_{\text{eff}}\frac{\partial u}{\partial x}-\frac{2}{3}\mu_{\text{eff}}\left(\frac{\partial u}{\partial x}+\frac{\partial v}{\partial y}+\frac{\partial w}{\partial z}\right)\right)+\frac{\partial}{\partial y}\left(\mu_{\text{eff}}\left(\frac{\partial u}{\partial y}+\frac{\partial v}{\partial x}\right)\right)+\frac{\partial}{\partial z}\left(\mu_{\text{eff}}\left(\frac{\partial u}{\partial z}+\frac{\partial w}{\partial x}\right)\right), \tag{2}$$

y momentum

$$\frac{\partial(\rho uv)}{\partial x}+\frac{\partial(\rho vv)}{\partial y}+\frac{\partial(\rho wv)}{\partial z}=-\frac{\partial p}{\partial y}+\frac{\partial}{\partial x}\left(\mu_{\text{eff}}\left(\frac{\partial u}{\partial y}+\frac{\partial v}{\partial x}\right)\right)+\frac{\partial}{\partial y}\left(2\mu_{\text{eff}}\frac{\partial v}{\partial y}-\frac{2}{3}\mu_{\text{eff}}\left(\frac{\partial u}{\partial x}+\frac{\partial v}{\partial y}+\frac{\partial w}{\partial z}\right)\right)+\frac{\partial}{\partial z}\left(\mu_{\text{eff}}\left(\frac{\partial v}{\partial z}+\frac{\partial w}{\partial y}\right)\right), \tag{3}$$

z momentum

$$\frac{\partial(\rho uw)}{\partial x}+\frac{\partial(\rho vw)}{\partial y}+\frac{\partial(\rho ww)}{\partial z}=-\frac{\partial p}{\partial z}+\frac{\partial}{\partial x}\left(\mu_{\text{eff}}\left(\frac{\partial u}{\partial z}+\frac{\partial w}{\partial x}\right)\right)+\frac{\partial}{\partial y}\left(\mu_{\text{eff}}\left(\frac{\partial v}{\partial z}+\frac{\partial w}{\partial y}\right)\right)+\frac{\partial}{\partial z}\left(2\mu_{\text{eff}}\frac{\partial w}{\partial z}-\frac{2}{3}\mu_{\text{eff}}\left(\frac{\partial u}{\partial x}+\frac{\partial v}{\partial y}+\frac{\partial w}{\partial z}\right)\right), \tag{4}$$

3. Energy equation

$$\frac{\partial(\rho uT)}{\partial x}+\frac{\partial(\rho vT)}{\partial y}+\frac{\partial(\rho wT)}{\partial z}=\frac{\partial}{\partial x}\left(\Gamma_{\text{eff}}\frac{\partial T}{\partial x}\right)+\frac{\partial}{\partial y}\left(\Gamma_{\text{eff}}\frac{\partial T}{\partial y}\right)+\frac{\partial}{\partial z}\left(\Gamma_{\text{eff}}\frac{\partial T}{\partial z}\right)+S_T\,, \tag{5}$$

where:

$$S_T = 0, \tag{6}$$

$$\mu_{\text{eff}} = \mu + \mu_t\,, \tag{7}$$

$$\Gamma_{\text{eff}} = \frac{\mu_{\text{eff}}}{\delta_{\text{eff}}} + \frac{\mu_t}{\delta_t}\,, \tag{8}$$

and δ_{eff} is the effective Prandtl number including the turbulent dynamic viscosity and turbulent diffusion coefficient.

For the turbulence effect, standard partial differential equations for a two-equation k-ε turbulence model which have the turbulent kinetic energy (k) and dissipation rate (ε) were considered in this study [36]. This model express the turbulent viscosity in terms of local values of k, ε and ρ as follow:

$$\mu_t = \frac{\rho C_\mu k^2}{\varepsilon}\,, \tag{9}$$

1. Turbulent kinetic energy (k):

$$\frac{\partial(\rho u k)}{\partial x} + \frac{\partial(\rho v k)}{\partial y} + \frac{\partial(\rho w k)}{\partial z} = \frac{\partial}{\partial x}\left(\Gamma_k \frac{\partial k}{\partial x}\right) + \frac{\partial}{\partial y}\left(\Gamma_k \frac{\partial k}{\partial y}\right) + \frac{\partial}{\partial z}\left(\Gamma_k \frac{\partial k}{\partial z}\right) + G - \varepsilon\,, \tag{10}$$

$$\Gamma_k = \frac{\mu_{\text{eff}}}{\delta_k}\,. \tag{11}$$

2. Dissipation rate (ε):

$$\frac{\partial(\rho u \varepsilon)}{\partial x} + \frac{\partial(\rho v \varepsilon)}{\partial y} + \frac{\partial(\rho w \varepsilon)}{\partial z} = \frac{\partial}{\partial x}\left(\Gamma_\varepsilon \frac{\partial \varepsilon}{\partial x}\right) + \frac{\partial}{\partial y}\left(\Gamma_\varepsilon \frac{\partial \varepsilon}{\partial y}\right) + \frac{\partial}{\partial z}\left(\Gamma_\varepsilon \frac{\partial \varepsilon}{\partial z}\right) + \frac{\varepsilon}{k}\left(C_1 G - C_2 \varepsilon\right), \tag{12}$$

where the values of constants C_μ, C_1, C_2, δ_k, δ_ε and δ_t are 0.09, 1.44, 1.92, 1.0, 1.3, and 0.9, respectively,

$$\Gamma_\varepsilon = \frac{\mu_{\text{eff}}}{\delta_e}\,. \tag{13}$$

Now, the governing equations can be written in the general form as follows:

$$\frac{\partial(\rho u \phi)}{\partial x} + \frac{\partial(\rho v \phi)}{\partial y} + \frac{\partial(\rho w \phi)}{\partial z} = \frac{\partial}{\partial x}\left[\Gamma_\phi \left(\frac{\partial \phi}{\partial x}\right)\right] + \frac{\partial}{\partial y}\left[\Gamma_\phi \left(\frac{\partial \phi}{\partial y}\right)\right] + \frac{\partial}{\partial z}\left[\Gamma_\phi \left(\frac{\partial \phi}{\partial z}\right)\right] + S_\phi\,, \tag{14}$$

where ϕ is the dependent variable while Γ_ϕ and S_ϕ are the diffusion coefficient and the source term, respectively.

By integrating equation (14) over the control volume, the result can be represented in a discretization form as:

$$a_P \phi_P = \sum_{nb} a_{nb} \phi_{nb} + S_\phi \,. \tag{15}$$

Utilizing hybrid difference scheme of Patankar [37], the discretization coefficients can be written as:

$$\begin{gathered} a_P = \sum_{nb} a_{nb} \,, \\ a_E = \max\left[-F_e, (D_e - 0.5F_e), 0\right], \quad a_W = \max\left[F_w, (D_w + 0.5F_w), 0\right], \\ a_N = \max\left[-F_n, (D_n - 0.5F_n), 0\right], \quad a_S = \max\left[F_s, (D_s + 0.5F_s), 0\right], \\ a_T = \max\left[-F_t, (D_t - 0.5F_t), 0\right], \quad a_B = \max\left[F_b, (D_b + 0.5F_b), 0\right], \end{gathered} \tag{16}$$

where F and D represent the strength of the convection and diffusion term for the control volume respectively.

SIMPLE algorithm is used to solve Navier-Stokes and energy equations, with uniform staggered grids were employed with 81, 51, 21 mesh in x, y, z, respectively.

3.2. Numerical modeling for heat transfer within a solid walls

$$\sum q_{\text{in all face}} = q_s + q_n + q_e + q_w + q_t + q_b \,, \tag{17}$$

$$\sum q_{\text{in all face}} = 0. \tag{18}$$

3.2.1. Upper Glass Cover

The solar radiation falling on the collector passes through the upper and middle glass panels and finally falls on the absorbing plate. Then, due to the presence of reflected rays for each of the two glass panels, the value of the solar radiation passing through the glass varies. To determine this, the radiation intensity was measured before and after the glass panel experimentally. Thus, the percentage of radiation transmitted from the upper glass panel to the middle is equal to 79% of the incident radiation, and the percentage of radiation transmitted through the middle glass panel to the absorber plate is 79% of the radiation transmitted from the upper glass plate. Thus, the percentage of radiation falling on the absorbing plate is equal to 62.41% of the total radiation.

Now, the thickness of solid surfaces such as upper or middle glass panels or absorber plate will be distributed to 3 mesh (layer) for each surface (upper, lower, intermediate). The mathematical model will be summarized as follows [38]:

For upper glass cover:
a) (upper surface)

$$\begin{aligned} a_e &= a_w = \frac{k_c a_x}{2\Delta x}\,, \qquad a_t = a_b = \frac{k_c a_z}{2\Delta z}\,, \\ a_n &= h_{\text{amb}} a_y\,, \qquad a_s = \frac{k_c a_y}{\Delta y}\,, \\ a_p &= a_e + a_w + a_n + a_s + a_t + a_b\,, \end{aligned} \tag{19}$$

$$\begin{aligned} T_{Ug(i,j,k)\text{new}} = T_{Ug(i,j,k)\text{old}}(1-\omega) + \omega\Big[& a_e T_{Ug(i+1,j,k)} + a_w T_{Ug(i-1,j,k)} \\ & + a_n T_{\text{amb}} + a_s T_{Ug(i,j-1,k)} + a_t T_{Ug(i,j,k+1)} \\ & + a_b T_{Ug(i,j,k-1)} + a_y q\Big]/a_p\,. \end{aligned} \tag{20}$$

b) intermediate layer between upper and lower surfaces

$$\begin{aligned} a_e &= a_w = \frac{k_c a_x}{\Delta x}\,, \quad a_n = a_s = \frac{k_c a_y}{\Delta y}\,, \quad a_t = a_b = \frac{k_c a_z}{\Delta z}\,, \\ a_p &= a_e + a_w + a_n + a_s + a_t + a_b\,, \end{aligned} \tag{21}$$

$$\begin{aligned} T_{Ug(i,J,k)\text{new}} = T_{Ug(i,J,k)\text{old}}(1-\omega) + \omega\Big[& a_e T_{Ug(i+1,j,k)} + a_w T_{Ug(i-1,j,k)} \\ & + a_n T_{Ug(i,j+1,k)} + a_s T_{Ug(i,j-1,k)} + a_t T_{Ug(i,j,k+1)} \\ & + a_b T_{Ug(i,j,k-1)} + a_y q\Big]/a_p\,. \end{aligned} \tag{22}$$

c) lower surface

$$\begin{aligned} a_e &= a_w = \frac{k_c a_x}{2\Delta x}\,, \qquad a_n = \frac{k_c a_y}{\Delta y}\,, \\ a_s &= h_a a_y\,, \qquad a_t = a_b = \frac{k_c a_z}{2\Delta z}\,, \\ a_p &= a_e + a_w + a_n + a_s + a_t + a_b\,, \end{aligned} \tag{23}$$

$$\begin{aligned} T_{Ug(i,J,k)\text{new}} = T_{Ug(i,J,k)\text{old}}(1-\omega) + \omega\Big[& a_e T_{Ug(i+1,j,k)} + a_w T_{Ug(i-1,j,k)} \\ & + a_n T_{Ug(i,j+1,k)} + a_s T_a + a_t T_{Ug(i,j,k+1)} + a_b T_{Ug(i,j,k-1)} \\ & + a_y q\Big]/a_p\,. \end{aligned} \tag{24}$$

In the same manner, the equations for the middle glass plate as well as the absorber plate can be written.

Now, to calculate the collector efficiency, the following equations can be adopted:

$$Q_u = \dot{m}\, c_p \left(T_{fo} - T_{f\text{in}}\right), \tag{25}$$

$$Q_i = G_S A_c, \tag{26}$$

$$\eta = \frac{Q_u}{Q_i}. \tag{27}$$

3.3. Boundary and initial conditions

At the entrance, the exit, and the walls, the boundary conditions will be described.

3.3.1. Boundary conditions at inlet

At the entrances to collector, all the variables (u, v, T, k, ε) must be specified. The inlet boundary condition can be written as:

$$\begin{gathered} u(0,y) = u_{\text{in}}, \quad v(0,y) = 0, \quad T(0,y) = T_{\text{in}}, \\ k(0,y) = k_{\text{in}} \quad \text{and} \quad \varepsilon(0,y) = \varepsilon_{\text{in}}, \end{gathered} \tag{28}$$

where:

$$k_{\text{in}} = C_k u_{\text{in}}^2, \tag{29}$$

$$\varepsilon_{\text{in}} = \frac{C_\mu k_{\text{in}}^{1.5}}{0.5 D_h C_\varepsilon}, \tag{30}$$

where C_k and C_ε are constants $C_k = 0.003$; $C_\varepsilon = 0.03$ [36].

3.3.2. Boundary conditions at exit

At the exit section of the collector, the normal gradients for all variable are set to be zero as follow:

$$\frac{\partial \phi}{\partial n} = 0, \quad \text{where} \quad \phi \ \text{is}: \ (u, v, T, k, \varepsilon). \tag{31}$$

3.3.3. Walls boundary conditions

When a flow is turbulent (at Ra > 109) and near the wall, the local Re is very low, as a result of this, turbulent viscosity is no longer dominant. The module of k-ε is invalid in this layers, thus individual treatment is needed to describe flow characteristics. This is known as the wall function [39].

In the solid walls (two glazing and metal absorber plates), the velocity components set are equal to zero.

4. Validity of the present code

In order to verify the reliability of the current numerical code, the code has been tested on a previous experimental study under the same operating conditions. Since the current collector is not commonly used and no previous research is available about it, the verification of the program was carried out on a traditional collector that contains an intermediate absorbent metal plate instead of the glass plate proposed in this study. Fig. 2 represents a comparison between present numerical results with those of experimental results reached by Jalil et al. [10]. This figure illustrates the relation between solar intensity with the average temperature out from collector. The results were identical with an error that does not exceed 0.4%.

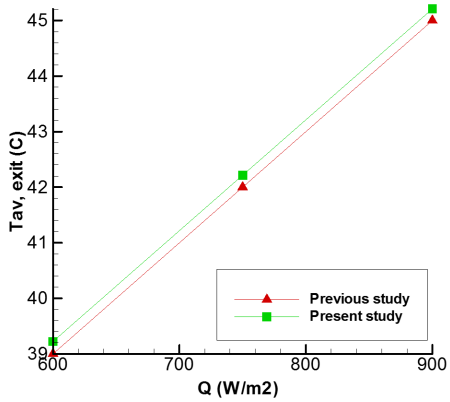

Fig. 2. Compression of present numerical results with previous experimental results, (Jalil et al. [10], traditional collector)

5. Results and discussions

Due to the reason that the current collector is not commonly used and in order to demonstrate the feasibility of its use, its performance was compared with that of the traditional collector that contains an absorbent metal plate in the middle and for three radiation intensity values (600, 750 and 900 W/m^2).

Fig. 3 shows the variation of T_{av} which represents average temperature in each channel section, with the flow direction of the traditional collector. From figures below, it is noted that there was an increase in T_{av} with the increase in radiation intensity and that the increase in forward (input channel) was greater than in backward (output channel) due to the fact that the emissivity and transmittance of glass was higher than that of metal. The increasing in T_{av} in input channel was about 33% while in the output channel was about 8.3%, while for hole collector from inlet to outlet was 44.4%.

Fig. 4 is similar to Fig. 3 but for the present collector where there is the same behavior of flow between the two figures except that there is an increase T_{av} in the present collector for all the radiation intensity ranges. The increase in T_{av} from inlet to outlet was 48.1%.

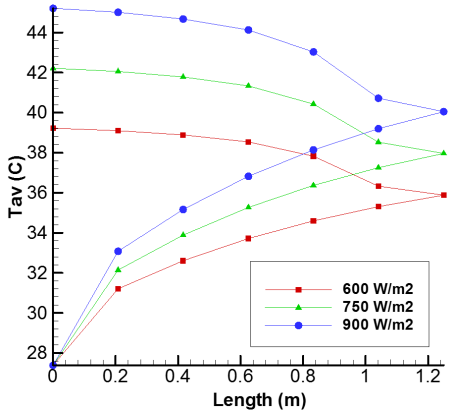

Fig. 3. Variation of average temperature from inlet to outlet for traditional collector

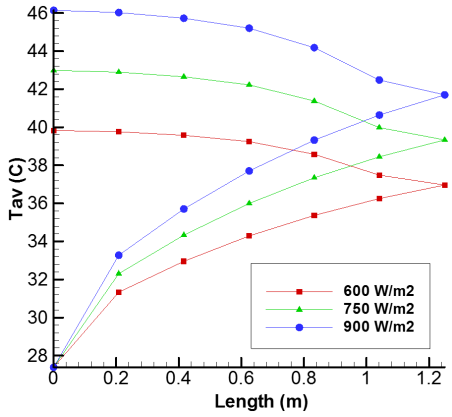

Fig. 4. Variation of average temperature from inlet to outlet for present collector

Figs 5–7 represent a comparison between the present collector and the conventional collector at each radiation intensity. From these figures, it can be noticed that the average temperature values are higher in the present collector than the traditional collector for all the radiation intensity ranges.

Fig. 5 illustrates the variation of T_{av} for the present and a traditional collector at 600 W/m^2 solar intensity. The increase in T_{av} from inlet to outlet was 48.1% for present collector while it was 44.4% for the traditional one.

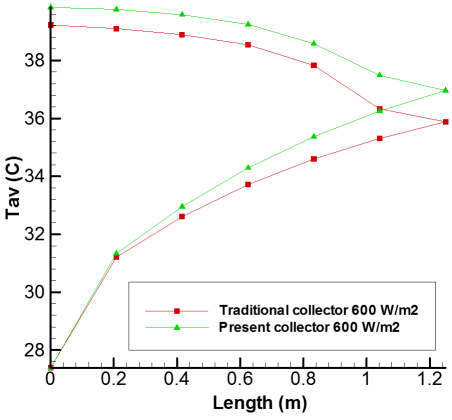

Fig. 5. Compression of T_{av} of present and traditional collector at 600 W/m^2 solar intensity

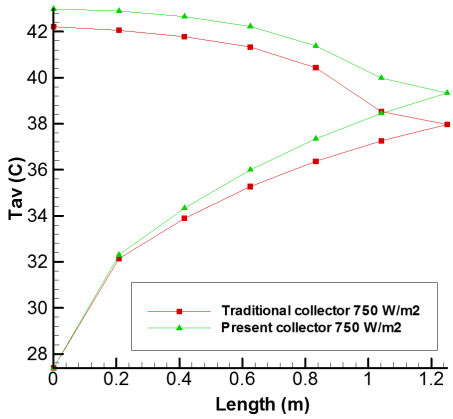

Fig. 6. Compression of T_{av} of present and traditional collector at 750 W/m^2 solar intensity

Fig. 6 shows the variation of T_{av} for the present and a traditional collector at 750 W/m^2 solar intensity. The increase in T_{av} from inlet to outlet was 59.2% for present collector while it was 55.5% for the traditional collector.

As for the radiation intensity of 900 W/m^2, the increase in T_{av} from inlet to outlet was 70.3% for present collector while it was 66.6% for the traditional collector, see Fig. 7.

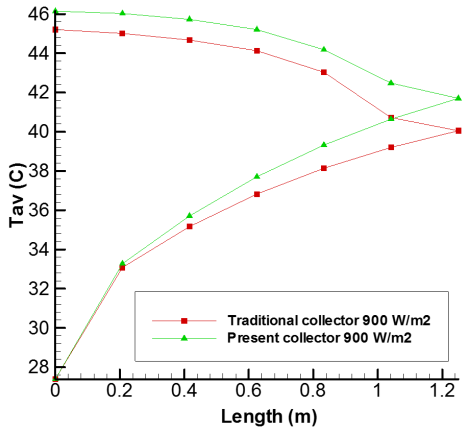

Fig. 7. Compression of T_{av} of present and traditional collector at 900 W/m^2 solar intensity

Fig. 8 illustrates the variation in average temperature at the exit of the collector with the variation in solar intensity for both collectors. As in the previous figures, it can be noticed that the present collector has a higher T_{av} at exit than the traditional collector with an increase rate of about 2.3%.

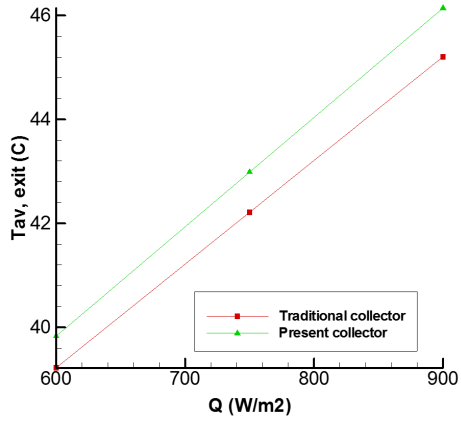

Fig. 8. Compression of T_{av} at exit for each solar intensity for present and traditional collector

Fig. 9 shows flow field for the present collector at 750 W/m^2 solar intensity. From this figure, it can be observed that the value of velocity profile is at the highest in the middle and it decreases near the walls until it becomes zero at the wall, as a result of the wall function. An increased in the velocity of flow for the lower passage was also observed.

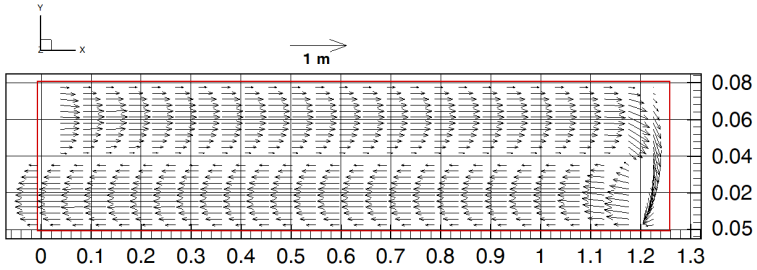

Fig. 9. Vector field for present collector at 750 W/m^2 solar intensity

While Fig. 10 illustrates the contour of temperature for the present collector for each solar intensity. The increase in temperature was clearly noticed with the increase in solar intensity. These figures were plotted with the same temperature levels settings, so it is clear that temperature values of the middle glass plate are being increased significantly with the increase in solar intensity and the effect on the air temperature near the glass in the upper and lower passages, in addition to the increase in the temperature of the absorbing plate, and this explains the increase in the air velocity value in the lower passage, which is showed in Fig. 9.

Table 1 illustrates compression of efficiency between the present and the traditional collector at each solar intensity. From this it can be noticed that the present collector is efficient than the traditional collector.

Table 1. Comparison of efficiency between present and traditional collectors

Type of collector	Solar intensity (W/m^2)	Collector efficiency
Present collector	600	0.529
	750	0.514
	900	0.503
Traditional collector	600	0.508
	750	0.492
	900	0.481

From the results, it can be seen that present novel collector is more efficient than that of a traditional design.

Now, as a parametric study for the present novel collector, the effect of changing the mass flow rate on the average temperature of the air outside this collector is

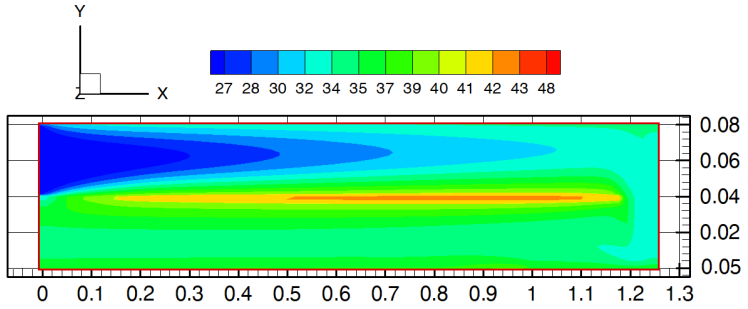

(a) 600 W/m^2 solar intensity

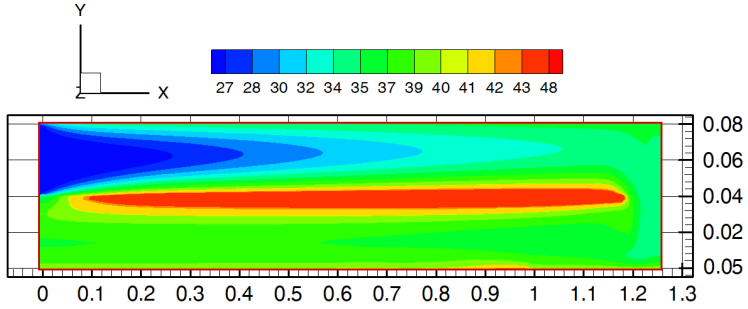

(b) 750 W/m^2 solar intensity

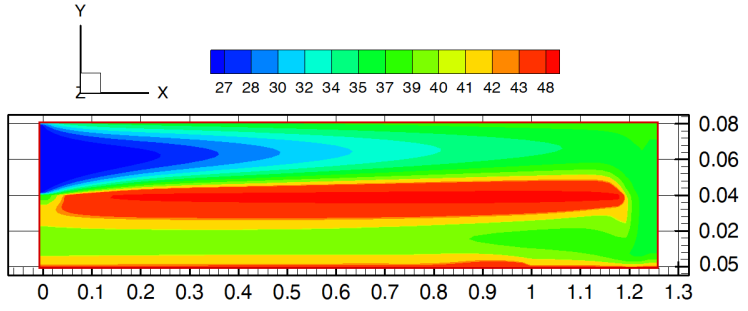

(c) 900 W/m^2 solar intensity

Fig. 10. Temperature contour for present collector at various solar intensity

studied. Three values of the mass flow rate will be studied (0.009, 0.018, 0.027) kg/s at solar intensity of 750 W/m^2, as in Fig. 11. From this figure it can be noticed that there is a decrease in average temperature rise with increasing mass flow rate, where rise in T_{av} was (0.59, 0.51 and 0.46)% at mass flow rate (0.009, 0.018 and 0.027) kg/s, respectively. This agreed with what was found by Ghritlahre [12] and Fudholi et al. [33].

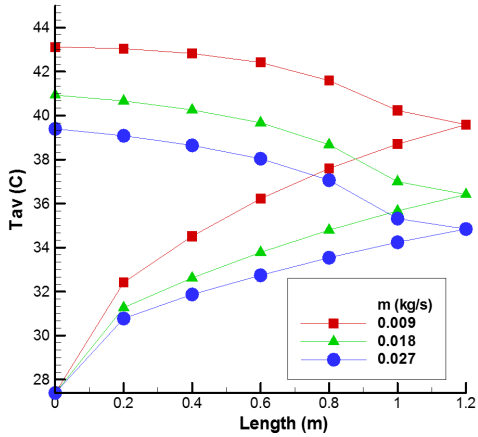

Fig. 11. Variation of average temperature from inlet to outlet for present collector at 750 W/m^2 solar inensity for three values of mass flowrate

6. Conclusions

The performance of double-pass solar air heater of newly proposed configuration is studied. The present proposed collector consists of middle glass plate instead of the middle metal absorber. A FORTRAN-90 program is built to simulate the mathematical model of double-pass solar air heater based on solving steady state two dimensional Navier-Stokes equations and energy equation based on the finite volume method. Turbulence effect is simulated by two equations k-ε module.

From the results, the following can be concluded:

1. In general, average temperature values were higher in the present collector than the traditional collector for all the radiation intensity ranges.
2. The difference in T_{av} from inlet to outlet for the present collector was higher by 8.3% than that of the traditional one at 600 W/m^2 solar intensity.
3. At solar intensity of 750 W/m^2, there was an increase of about 6.6% in Tav for the present collector over that of the traditional collector.
4. At solar intensity of 900 W/m^2, the increase in T_{av} was 5.5% over that of the traditional collector.
5. At collector exit, there was an increase in T_{av} for the present collector by 2.3% over that of the traditional collector for all solar intensity.
6. There was an increase in efficiency for the present collector over that of the traditional one of about 1.04 for all solar intensity range, while there was a decrease in T_{av} and thus efficiency, with the increase in mass flow rate.

From the foregoing, it can be concluded that the proposed novel collector is more efficient than its traditional counterpart and can be considered in the practical applications.

References

[1] J.M. Jalil, A.H. Ayaal, and A.A. Hardan. Numerical investigation of thermal performance for air solar collector with multi inlets. *IOP Conference Series: Materials Science and Engineering*, 765:012036, 2020. doi: 10.1088/1757-899X/765/1/012036.

[2] A. Abene,V. Dubois, M. Le Ray, and A. Ouagued. Study of a solar air flat plate collector: use of obstacles and application for the drying of grape. *Journal of Food Engineering*, 65(1):15–22, 2004. doi: 10.1016/j.jfoodeng.2003.11.002.

[3] R.S. Gill, S. Singh, and P.P. Singh. Low cost solar air heater. *Energy Conversion and Management*, 57:131–142, 2012. doi: 10.1016/j.enconman.2011.12.019.

[4] A.E. Kabeel, A. Khalil, S.M. Shalaby, and M.E. Zayed. Experimental investigation of thermal performance of flat and v-corrugated plate solar air heaters with and without PCM as thermal energy storage. *Energy Conversion and Management*, 113:264–772, 2016. doi: 10.1016/j.enconman.2016.01.068.

[5] A. Sakhrieh and A. Al-Ghandoor. Experimental investigation of the performance of five types of solar collectors. *Energy Conversion and Management*, 65:715–720, 2013. doi: 10.1016/j.enconman.2011.12.038.

[6] J.M. Jalil, K.F. Sultan, and L.A. Rasheed. Numerical and experimental investigation of solar air collectors performance connected in series. *Engineering and Technology Journal*, 35(3):190–196, 2017.

[7] J. Assadeg J, A.H.A. Al-Waeli, A. Fudholi, and K. Sopian. Energetic and exergetic analysis of a new double pass solar air collector with fins and phase change material. *Solar Energy*, 226:260–271, 2021. doi: 10.1016/j.solener.2021.08.056.

[8] J.M. Jalil and S.J. Ali. Thermal investigations of double pass solar air heater with two types of porous media of different thermal conductivity. *Engineering and Technology Journal*, 39(1):79–88, 2021. doi: 10.30684/etj.v39i1A.1704.

[9] S. Bassem, J.M. Jalil, and S.J. Ismael. Experimental study of double pass water passage in evacuated tube with parabolic trough collector. *Journal of Physics: Conference Series*, 1973:012058, 2021. doi: 10.1088/1742-6596/1973/1/012058.

[10] J.M. Jalil, R.F. Nothim, and M.M. Hameed. Effect of wavy fins on thermal performance of double pass solar air heater. *Engineering and Technology Journal*, 39(9):1362–1368, 2021. doi: 10.30684/etj.v39i9.1775.

[11] W. Siddique, A. Raheem, M. Aqeel, S. Qayyum, T, Salamen, K. Waheed, and K. Qureshi. Evaluation of thermal performance factor for solar air heaters with artificially roughened channels. *Archive of Mechanical Engineering*, 68(2):195–225, 2021. doi: 10.24425/ame.2021.137048.

[12] H.K. Ghritlahre. An experimental study of solar air heater using arc shaped wire rib roughness based on energy and exergy analysis. *Archives of Thermodynamics*. 42(3):115–139, 2021. doi: 10.24425/ather.2021.138112.

[13] A. Kumar, Akshayveer, A.P. Singh, and O.P. Singh. Efficient designs of double-pass curved solar air heaters. *Renewable Energy*, 160:1105–1118, 2020. doi: 10.1016/j.renene.2020.06.115.

[14] S. Abo-Elfadl, H. Hassan, and M.F. El-Dosoky. Study of the performance of double pass solar air heater of a new designed absorber: An experimental work. *Solar Energy*, 198:479–489, 2020. doi: 10.1016/j.solener.2020.01.091.

[15] S. Singh. Experimental and numerical investigations of a single and double pass porous serpentine wavy wiremesh packed bed solar air heater. *Renewable Energy*, 145:1361–1387, 2020. doi: 10.1016/j.renene.2019.06.137.

[16] H.K. Ghritlahre and P.K. Sahu. A comprehensive review on energy and exergy analysis of solar air heaters. *Archives of Thermodynamics*. 41(3):183–222, 2020. doi: 10.24425/ather.2020.134577.

[17] S. Dogra, R.D. Jilte, and A. Sharma. Study of performance enhancement of single and double pass solar air heater with change in surface roughness. *Journal of Physics: Conference Series*, 1531:012091, 2020. doi: 10.1088/1742-6596/1531/1/012091.

[18] S. Sivakumar, K. Siva, and M. Mohanraj. Experimental thermodynamic analysis of a forced convection solar air heater using absorber plate with pin-fins. *Journal of Thermal Analysis and Calorimetry*, 136(1):39–47, 2019. doi: 10.1007/s10973-018-07998-5.

[19] S.M. Salih J.M. Jalil, and S.E. Najim. Experimental and numerical analysis of double-pass solar air heater utilizing multiple capsules PCM. *Renewable Energy*, 143:1053–1066, 2019. doi: 10.1016/j.renene.2019.05.050.

[20] S. Singh, L. Dhruw, and S. Chander. Experimental investigation of a double pass converging finned wire mesh packed bed solar air heater. *Journal of Energy Storage*, 21:713–723, 2019. doi: 10.1016/j.est.2019.01.003.

[21] P.T. Saravanakumar, D. Somasundaram, and M.M. Matheswaran. Thermal and thermo-hydraulic analysis of arc shaped rib roughened solar air heater integrated with fins and baffles. *Solar Energy*, 180:360–371, 2019. doi: 10.1016/j.solener.2019.01.036.

[22] C.A. Komolafe, I.O. Oluwaleye, O. Awogbemi, and C.O. Osueke. Experimental investigation and thermal analysis of solar air heater having rectangular rib roughness on the absorber plate. *Case Studies in Thermal Engineering*, 14:100442, 2019. doi: 10.1016/j.csite.2019.100442.

[23] H. Mzad, K. Bey, and R. Khelif. Investigative study of the thermal performance of a trial solar air heater. *Case Studies in Thermal Engineering*, 13:100373, 2019. doi: 10.1016/ j.csite. 2018.100373.

[24] S.S. Patel and A. Lanjewar. Exergy based analysis of solar air heater duct with W-shaped rib roughness on the absorber plate. *Archives of Thermodynamics*, 40(4):21–48, 2019. doi: 10.24425/ather.2019.130006.

[25] A.S. Mahmood. Experimental study on double-pass solar air heater with and without using phase change material. *Journal of Engineering*. 25(2):1-17. doi: 10.31026/j.eng.2019.02.01.

[26] R.K. Ravi and R.P. Saini. Effect of roughness elements on thermal and thermohydraulic performance of double pass solar air heater duct having discrete multi V-shaped and staggered rib roughness on both sides of the absorber plate. *Experimental Heat Transfer*, 31(1):47–67, 2018. doi: 10.1080/08916152.2017.1350217.

[27] H. Hassan and S. Abo-Elfadl. Experimental study on the performance of double pass and two inlet ports solar air heater (SAH) at different configurations of the absorber plate. *Renewable Energy*, 116:728–740, 2018. doi: 10.1016/j.renene.2017.09.047.

[28] S.S. Hosseini, A. Ramiar, and A.A. Ranjbar. Numerical investigation of natural convection solar air heater with different fins shape. *Renewable Energy*, 117:488–500, 2018. doi: 10.1016/ j.renene. 2017.10.052.

[29] A.P. Singh and O.P. Singh. Performance enhancement of a curved solar air heater using CFD. *Solar Energy*, 174:556–569, 2018. doi: 10.1016/j.solener.2018.09.053.

[30] A.M. Rasham and M.M.M. Alaskari. Thermal analysis of double-pass solar air collector with different materials of absorber plate and different dimensions of air channels. *International Journal of Science and Research (IJSR)*, 6(8):901–908, 2017.

[31] R. Kumar and P. Chand. Performance enhancement of solar air heater using herringbone corrugated fins. *Energy*, 127:271–279, 2017. doi: 10.1016/j.energy.2017.03.128.

[32] M.W. Kareem, K. Habib, and S.A. Sulaiman. Comparative study of single pass collector and double pass solar collector filled with porous media. *Asian Journal of Scientific Research*, 6(3):445–455, 2013. doi: 10.3923/ajsr.2013.445.455.

[33] A. Fudholi, M.H. Ruslan, M.Y. Othman, M. Yahya, S. Supranto, A. Zaharim, and K. Sopian. Collector efficiency of the double-pass solar air collectors with fins. In *Proceedings of the 9th WSEAS International Conference on System Science and Simulation in Engineering*, pages 428–434, Japan, 2010.

[34] B.M. Ramani, A. Gupta, and R. Kumar. Performance of a double pass solar air collector. *Solar Energy*, 84(11):1929–1937, 2010. doi: 10.1016/j.solener.2010.07.007.

[35] H.K. Versteeg and W. Malalsekera. *An Introduction to Computational Fluid Dynamics. The Finite Volume Method*. Pearson Education Ltd. 1995.

[36] B.E. Launder and D.B. Spalding. The numerical computation of turbulent flows. In S.V. Patankar, A. Pollard, A.K. Singhal, and S.P. Vanka, editors: *Numerical Prediction of Flow, Heat Transfer, Turbulence and Combustion*, pages 96–116. Pergamon, 1983. doi: 10.1016/B978-0-08-030937-8.50016-7.

[37] S.V. Patankar. *Numerical Heat Transfer and Fluid Flow*. CRC Press, 2018. doi: 10.1201/9781482234213.

[38] N.I. Dawood, J.M. Jalil, and M.K. Ahmed. Experimental investigation of a window solar air collector with circular-perforated moveable absorber plates. *Journal of Physics: Conference Series*, 1973:012057, 2021. doi: 10.1088/1742-6596/1973/1/012057.

[39] F. Haghighat, Z. Jiang, J.C.Y. Wang, and F. Allard. Air movement in buildings using computational fluid dynamics. *Journal of Solar Energy Engineering*, 114(2):84–92, 1992. doi: 10.1115/1.2929994.